




Hydrogen storage thermodynamics and dynamics of La–Mg–Ni-based LaMg₁₂-type alloys synthesized by mechanical milling

Yang-Huan Zhang* , Peng-Fei Gong, Long-Wen Li, Hao Sun, Dian-Chen Feng, Shi-Hai Guo

Received: 4 December 2015 / Revised: 25 January 2016 / Accepted: 4 December 2016 / Published online: 5 January 2017
© The Nonferrous Metals Society of China and Springer-Verlag Berlin Heidelberg 2017

Abstract Nanocrystalline/amorphous LaMg₁₂-type alloy–Ni composites with a nominal composition of LaMg₁₁Ni + *x* wt% Ni (*x* = 100, 200) were synthesized by mechanical milling. Effects of Ni content and milling time on the gaseous hydrogen storage thermodynamics and dynamics of alloys were systematically investigated. The hydrogen desorption properties were studied by Sievert apparatus and a differential scanning calorimeter (DSC). Thermodynamic parameters (ΔH and ΔS) for the hydrogen absorption and desorption of alloys were calculated by Van't Hoff equation. Hydrogen desorption activation energy of alloy hydride was estimated by Arrhenius and Kissinger methods. The increase in Ni content has a slight effect on the thermodynamic properties of alloys, but it significantly enhances the hydrogen absorption and desorption kinetics performance of alloys. Moreover, variation of milling time clearly affects the hydrogen storage properties of alloys. Hydrogen absorption capacity (C_{100}^a) and hydrogen absorption saturation ratio (R_{10}^a) (a ratio of the hydrogen absorption capacity at 10 min to the saturated hydrogen absorption capacity) have maximum values with milling time varying. But hydrogen desorption ratio (R_{20}^d) (a ratio of the hydrogen desorption capacity at 20 min to the saturated hydrogen absorption capacity) always increases with milling time prolonging. Particularly,

prolonging milling time from 5 to 60 h makes R_{20}^d increase from 10.89% to 16.36% for the *x* = 100 alloy and from 13.93% to 21.68% for the *x* = 200 alloy, respectively.

Keywords LaMg₁₂ alloy; Mechanical milling; Thermodynamics and dynamics; Activation energy; Hydrogen storage

1 Introduction

As a globally accepted clean and recyclable fuel, hydrogen applied to vehicles fuel cell or portable electronic devices is a pursuit and dream of scientists around the world for decades. It is believed that the wide application of fuel cell vehicles will fundamentally cut down both energy consumption and carbon dioxide emissions due to the fact that about one-quarter of total energy in the world was consumed by transport [1]. A key technical challenge for the realization of onboard fuel cell or hydrogen-fueled vehicles is to develop a practical hydrogen storage system [2]. Among hydrogen storage methods, hydrogen storage in metal hydrides is considered to be one of the most promising alternatives to meet the requirements for mobile application [3]. Many hydrogen storage materials have been reported for the application goal, yet unfortunately none of them can meet all the requirements of the performance proposed by US Department of Energy (DOE) for vehicular applications [4, 5]. With regard to the hydrogen absorption capacity, Mg-based alloys are considered to be one of the most attractive candidates for hydrogen fuel cell vehicle. Particularly, RE-Mg₁₂-type Mg-based alloys have received considerable attention due to its gaseous hydrogen storage capacity of 3.7 wt%–6.0 wt% [6] and theoretical

Y.-H. Zhang*, P.-F. Gong, L.-W. Li, H. Sun, D.-C. Feng
Key Laboratory of Integrated Exploitation of Bayan Obo Multi-Metal Resources, Inner Mongolia University of Science and Technology, Baotou 014010, China
e-mail: zhangyh59@sina.com

Y.-H. Zhang, S.-H. Guo
Department of Functional Material Research, Central Iron and Steel Research Institute, Beijing 100081, China

electrochemical capacity (over 1000 mA·h·g⁻¹) [7], much higher than that of Mg–Ni alloy. However, their extremely low electrochemical discharge capacity at room temperature as well as quite poor cycle stability, and relatively high hydrogen desorption temperatures as well as sluggish hydriding/dehydriding kinetics, gravely hinder the practical application either as the negative electrode materials of Ni–MH battery or as the hydrogen storage materials of onboard use for the alloys. Therefore, how to improve the hydrogen storage kinetics of RE–Mg-based alloys is still a major challenge for the researchers in this area.

Generally, the primary principles for improving the hydrogen storage kinetics of RE–Mg-based alloys are believed to be no more than two categories: the first one is preparing an ultra-fine microstructure (sub-100 nm range); the second one is adding catalytic elements such as transition metals, transition metal oxides and rare-earth (RE) metals [8, 9]. Some methods, such as mechanical milling [10], melt spinning [11], physical vapor deposition [12], equal-channel angular pressing [13] and hydriding combustion synthesis [14], can be applied to prepare amorphous and nanocrystalline RE–Mg-based alloys with different compositions. Mechanical milling and melt spinning, in particular, are universally accepted techniques for obtaining amorphous and/or nanocrystalline alloys. Zhang et al. [15] reported that the as-spun Mg₁₀NiR (R = La, Nd and Sm) alloys displayed superior hydriding and dehydriding kinetics as a result of adding different rare-earth elements. Wang et al. [16] investigated the electrochemical hydrogen storage properties of ball-milled MmMg₁₂ alloy with Ni powders, and the results indicated that as Ni content in the alloy increased from 150 to 200 wt%, the first discharge capacity of the ball-milled sample increased from 770 to 1200 mA·h·g⁻¹. Yartys et al. reported that the LaMg₁₁Ni alloy solidified at the highest cooling rate exhibited the fastest hydrogenation kinetics, reaching maximum hydrogenation capacity of 5.02 wt% H [17]. Cao et al. [18] reported that the dehydrogenation enthalpy change and activation energy of Mg₈₅In₅Al₅Ti₅ alloy synthesized by plasma milling are lowered to 65.2 and 125.2 kJ·mol⁻¹, respectively.

It is well known that Ni can promote the amorphization process in the alloy and exert a highly powerful catalytic action on the hydrogen absorption and desorption of RE–Mg-based alloys, and hence, in the present work, Mg in the LaMg₁₂-type alloy was partially substituted by Ni. The nanocrystalline and amorphous LaMg₁₁Ni + *x* wt% Ni (*x* = 100, 200) alloys were prepared by mechanical milling, and the effects of Ni content and milling time on the gaseous hydrogen storage thermodynamics and kinetics performance of the alloys were investigated in detail.

2 Experimental

Experimental alloys with a chemical composition of LaMg₁₁Ni were prepared using a vacuum induction furnace in a helium atmosphere at a pressure of 0.04 MPa to prevent Mg from volatilization. A part of the as-cast alloys was mechanically crushed into powder with diameter of <50 μm. The alloy powder was mixed with carbonyl nickel powder with a weight ratio of 1:1 and 1:2, respectively. Subsequently, the mixed powder was mechanically milled by a planetary-type mill in an argon atmosphere to prevent the powder from oxidation during ball milling. The obtained samples were handled in a glove box under Ar atmosphere. Cr–Ni stainless steel ball and powder with a weight ratio of 35:1 were placed into Cr–Ni stainless steel vials together. Duration time was 5, 10, 20, 40 and 60 h, respectively. Milling speed was 135 r·min⁻¹.

Phase structures of as-cast and milled alloys before and after hydriding were determined using X-ray diffractometer (XRD, D/max/2400), which was performed with Cu Kα1 radiation filtered by graphite at 160 mA, 40 kV and 10 (°)·min⁻¹. The powder samples of the as-milled alloys were observed by high-resolution transmission electron microscope (HRTEM, JEM-2100F, operated at 200 kV), and their crystalline states were ascertained by electron diffraction (ED).

The hydrogen absorption and desorption kinetics and pressure–composition isotherms (P–C–T) curves of the alloys were measured by an automatically controlled Sieverts apparatus with a furnace controlled to an accuracy of ±1 K. The hydrogen absorption and desorption were, respectively, performed at 3 MPa hydrogen pressure (in fact, this pressure is the initial pressure of hydriding process) and 1 × 10⁻⁴ MPa at 553, 573, 593 and 613 K. 300 mg sample was loaded into a cylindrical reactor for each measurement.

Hydrogen desorption properties were also measured by differential scanning calorimeter (DSC, STA449C) at heating rates of 5, 10, 15 and 20 K·min⁻¹.

3 Results and discussion

3.1 Microstructural characteristics

The phase components and structure characteristics of as-cast and milled LaMg₁₁Ni + *x* wt% Ni (*x* = 0, 100, 200) alloys before and after hydriding were subjected to XRD detections, just as demonstrated in Fig. 1. It indicates that the as-cast LaMg₁₁Ni alloy contains a major phase La₂Mg₁₇ and a secondary phase Mg₂Ni. The mechanical milling results in the diffraction peaks merging and broadening with the increase in Ni content, suggesting that the crystalline structure has transformed to a nanocrystalline or amorphous structure. Furthermore, increasing Ni

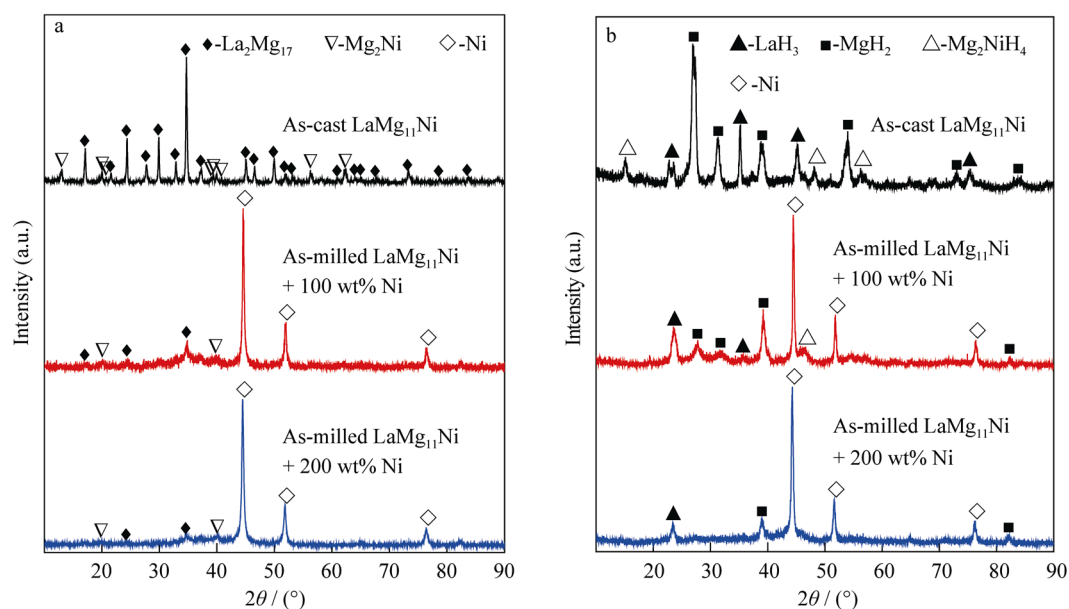


Fig. 1 XRD patterns of as-cast and milled (5 h) LaMg₁₁Ni + x wt% Ni ($x = 0, 100, 200$) alloys **a** before and **b** after hydriding

content in alloys evidently lowers the intensity of diffraction peaks and clearly broadens its width, implying that increasing Ni content promotes the formation of glass in the alloy. As stated by Abdellaoui et al. [19], the increase in Ni content can lower the activation energy for the crystalline to amorphous phase transformation of the La–Mg alloys. After hydriding, three hydrides appear in the as-cast alloy, namely LaH₃, MgH₂ and Mg₂NiH₄, which originate from the following reactions [20]:



It can be found that the diffraction peaks of the hydrides clearly broaden, which is ascribed to the lattice stress and strain originated from hydrogen atoms entering into lattice interstitials.

Moreover, the detail information of as-cast LaMg₁₁Ni alloy also was analyzed according to the Rietveld refinements, as shown in Fig. 2. The milled alloys and hydrogenated alloys cannot be fitted with the Rietveld method because their XRD detections are amorphous. The as-cast LaMg₁₁Ni alloy is composed of major phase La₂Mg₁₇ (79.9 wt%) with space group of *P63/mmc* hexagonal structure ($a = b = 1.0342$ nm, $c = 1.0287$ nm) and secondary phase Mg₂Ni (21.1 wt%) with space group of *P6222* hexagonal structure ($a = b = 0.5209$ nm, $c = 1.3269$ nm).

Figure 3 shows HRTEM images and ED patterns of as-milled LaMg₁₁Ni + x wt% Ni ($x = 100, 200$) alloys. Two phases La₂Mg₁₇ and Mg₂Ni are found in the as-cast alloy, which is also supported by ED pattern. After milled for 5 h, the $x = 100$ alloy exhibits a major nanocrystalline

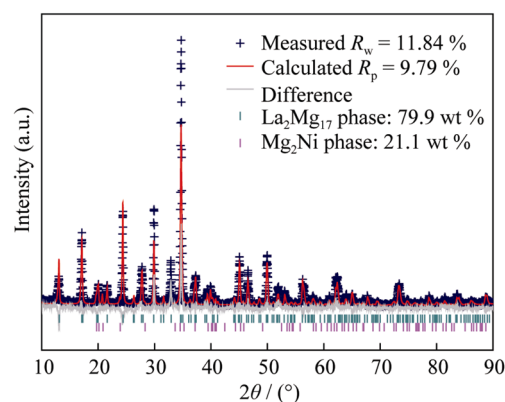


Fig. 2 Rietveld refinement on XRD patterns of as-cast LaMg₁₁Ni alloy (R_w , mathematical fitting coefficient; R_p , physical fitting coefficient)

structure, while the $x = 200$ alloy presents a visible nanocrystalline and amorphous structure, and the average size of the as-milled alloys measured by linear intercept method is found to be in the range of 8–12 nm. Meanwhile, some crystal defects, such as dislocation, grain boundary and twin, can be clearly observed in the as-milled alloys.

3.2 Gaseous hydrogen absorption/desorption thermodynamics

P–C–T curves of as-milled LaMg₁₁Ni + x wt% Ni ($x = 100, 200$) alloys are depicted in Fig. 4. Compared with the P–C–T curve of as-cast LaMg₁₁Ni alloys (not shown here), the absorption and desorption pressure plateaus of as-milled LaMg₁₁Ni + x wt% Ni ($x = 100, 200$) alloys are found to display a clear inclination and a large

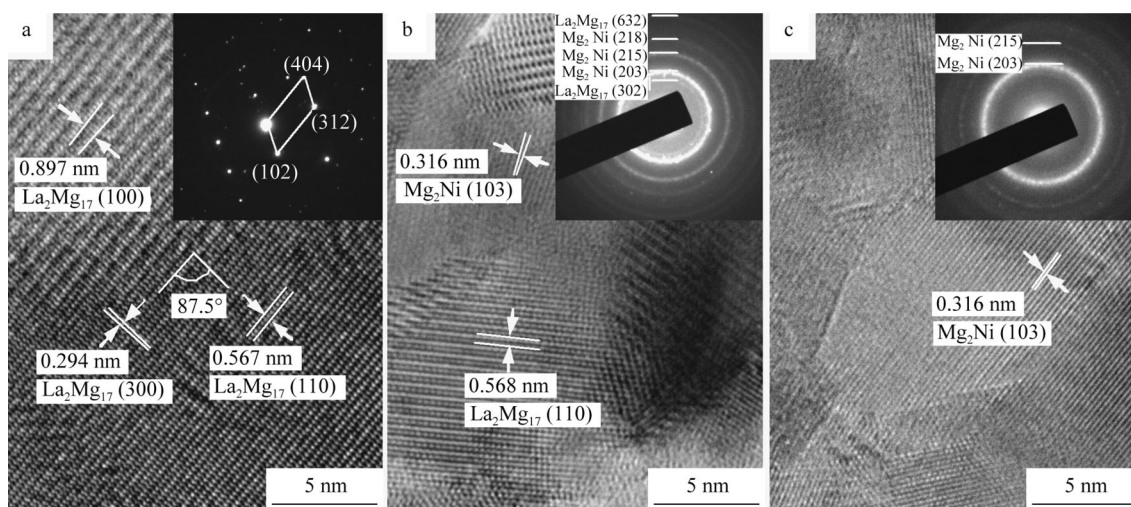


Fig. 3 HRTEM images and ED patterns of as-cast and milled (5 h) LaMg₁₁Ni + *x* wt% Ni (*x* = 0, 100, 200) alloys: **a** *x* = 0, **b** *x* = 100 and **c** *x* = 200

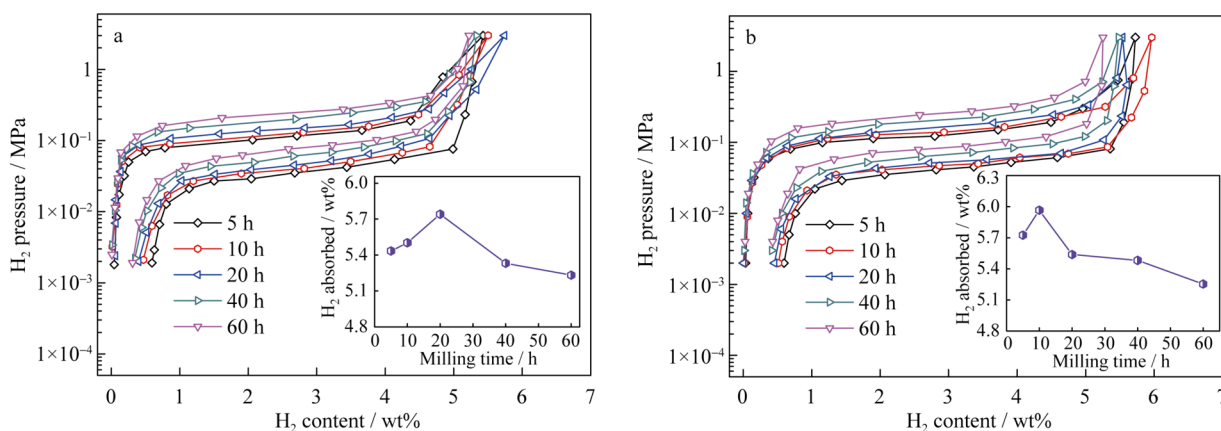


Fig. 4 P–C–T curves of as-milled LaMg₁₁Ni + *x* wt% Ni (*x* = 100, 200) alloys at 553 K: **a** *x* = 100 and **b** *x* = 200

hysteresis, suggesting that the addition of Ni and mechanical milling could also affect the desorption thermodynamic behavior of the alloys. The effect of milling and Ni addition brings on gentle tilted plateaus of MgH₂ and Mg₂NiH₄. The content of MgH₂ is much larger than that of Mg₂NiH₄; hence, MgH₂ shows a longer tilted plateaus, which may smoothly connect to the shorter tilted platform of Mg₂NiH₄. Therefore, it is shown only one plateau for P–C–T curves. Moreover, it is visible that the milling time has an evident effect on the maximum hydrogen storage capacities of the alloys. The milling time dependence of maximum hydrogen storage capacities is also shown in Fig. 4. Evidently, the hydrogen storage capacities of the alloys first augment and then decline with milling time prolonging, and the maximum value is 5.74% and 5.97% for *x* = 100 and 200 alloys, respectively, indicating that increasing Ni content conduces to the hydrogen absorption of the as-milled alloys. It is worth noting that the milling time corresponding to the

maximum hydrogen storage capacity clearly shortens with Ni content increasing.

To obtain the thermodynamic parameters (enthalpy change, ΔH , and entropy change, ΔS) of the hydrogen absorption/desorption reaction, P–C–T curves of as-milled (5 h) LaMg₁₁Ni + *x* wt% Ni (*x* = 100, 200) alloys were measured in the temperature range of 553–613 K, as shown in Fig. 5. From the data in Fig. 5, Van't Hoff diagrams can be obtained for the hydrogen absorption/desorption of the alloys (Fig. 5). Obviously, there are good linear relations between $\ln(p_{\text{H}_2}/p_0)$ and $1/T$ for all the alloys. Thus, the ΔH and ΔS can be easily calculated from Van't Hoff equation [21]:

$$\ln(p_{\text{H}_2}/p_0) = \frac{\Delta H}{RT} - \frac{\Delta S}{R} \quad (3)$$

where p_{H_2} is the equilibrium hydrogen gas pressure (due to the fact that the pressure plateaus have a clear inclination and, hence, it was taken the pressure corresponding to the

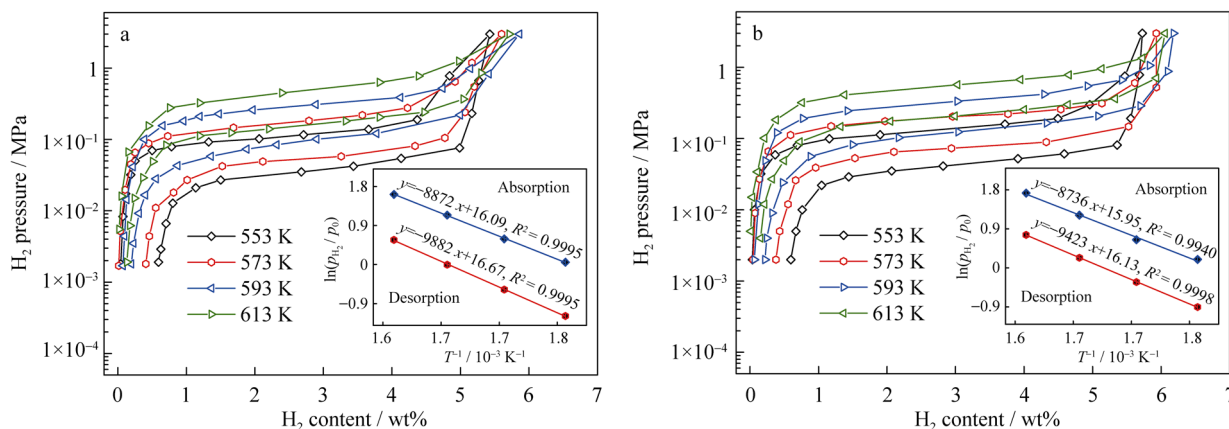


Fig. 5 P–C–T curves of as-milled (5 h) $\text{LaMg}_{11}\text{Ni} + x \text{ wt\% Ni}$ ($x = 100, 200$) alloys in a temperature range of 553–613 K and Van't Hoff diagrams for hydrogen absorption/desorption of alloys (R^2 , degree of fitting): **a** $x = 100$ and **b** $x = 200$

50% of the maximum hydrogen absorption/desorption capacity as equilibrium hydrogen gas pressure), p_0 is the standard atmospheric pressure, T is the sample temperature and R is the gas constant. The obtained enthalpy and entropy changes in the as-milled alloys are listed in Table 1. Apparently, increasing Ni content slightly affects the thermodynamic properties of the as-milled alloys.

3.3 Hydrogen absorption/desorption kinetics

Hydrogen absorption kinetics of alloys was evaluated by hydrogen absorption saturation ratio (R_t^a), defined as:

$$R_t^a = C_t^a / C_{100}^a \times 100\% \quad (4)$$

where C_{100}^a and C_t^a are hydrogen absorption capacities at the time of 100 min and t min, respectively. Apparently, for a fixed time (t), a larger saturation ratio (R_t^a) implies better hydrogen absorption kinetics. The experimental results show that the C_{100}^a values of all the experimental alloys exceed 98% of their saturated hydrogen absorption capacities. Hence, the C_{100}^a value is chosen as the saturated hydrogen absorption capacity of the alloy. Equally, the hydrogen desorption kinetics of alloys was symbolized by hydrogen desorption ratio (R_t^d), defined as:

$$R_t^d = C_t^d / C_{100}^a \times 100\% \quad (5)$$

where C_{100}^a is the hydrogen absorption capacity at 100 min and C_t^d is the hydrogen desorption capacity at the time of t

min. For a better mutual comparison, 10 min was taken as a benchmark for hydrogen absorption and 20 min was chosen for hydrogen absorption. Based on the above-mentioned definitions, the relationship can be established between R_{10}^a ($t = 10$) as well as R_{20}^d ($t = 20$) values of as-milled $\text{LaMg}_{11}\text{Ni} + x \text{ wt\% Ni}$ ($x = 100, 200$) alloys and the milling time, as displayed in Fig. 6. Clearly, R_{10}^a values of the as-milled alloys first increase and then decrease with milling time increasing. As milling time is 20 h for $x = 100$ alloy and 10 h for $x = 200$ alloy, R_{10}^a values of $\text{LaMg}_{11}\text{Ni} + x \text{ wt\% Ni}$ ($x = 100, 200$) alloys reach maximum, namely 83.2% and 92.3%, respectively. Differing from the hydrogen absorption kinetics, increasing milling time always benefits to improve the dehydrogenating kinetics of alloys. To be specific, milling time varying from 5 to 60 h gives rise to R_{20}^d value increasing from 10.89% to 16.36% for $x = 100$ alloy and from 13.93% to 21.68% for $x = 200$ alloy, respectively. Furthermore, it is noteworthy that, for the same milling time, $x = 200$ alloy displays a much higher R_{10}^a and R_{20}^d values, indicating that increasing Ni content generates relatively catalytic alloy surface for hydrogen reactions in the process of ball milling, as stated by Anik et al. [22].

Figure 7 describes the reaction time dependence of hydrogen desorption capacities of as-milled (5 h) $\text{LaMg}_{11}\text{Ni} + x \text{ wt\% Ni}$ ($x = 100, 200$) alloys in the temperature range of 553–613 K. It is evident that the hydrogen desorption kinetics is very intensive to temperature.

Table 1 Enthalpy and entropy change in as-milled (5 h) $\text{LaMg}_{11}\text{Ni} + x \text{ wt\% Ni}$ ($x = 100, 200$) alloys

LaMg ₁₁ Ni + x wt% Ni	Absorption		Desorption	
	$\Delta H/(\text{kJ}\cdot\text{mol}^{-1})$	$\Delta S/(\text{J}\cdot\text{mol}^{-1}\cdot\text{K}^{-1})$	$\Delta H/(\text{kJ}\cdot\text{mol}^{-1})$	$\Delta S/(\text{J}\cdot\text{mol}^{-1}\cdot\text{K}^{-1})$
$x = 100$	-73.35	-133.8	82.16	138.8
$x = 200$	-72.63	-132.6	78.34	134.1

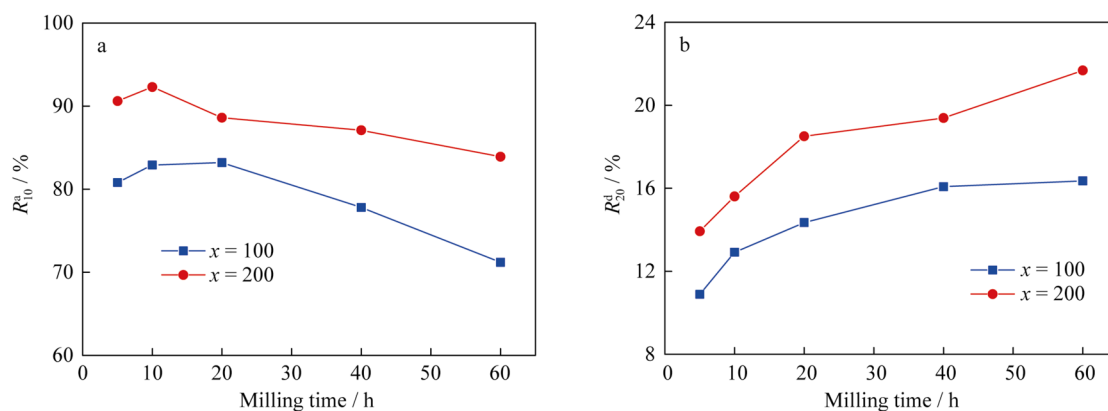


Fig. 6 Evolutions of **a** R_{10}^d and **b** R_{20}^d values of as-milled LaMg₁₁Ni + x wt% Ni ($x = 100, 200$) alloys at 553 K with milling time

More specifically, increasing hydrogen desorption temperature makes the dehydriding rate faster and the dehydriding capacity higher. By comparing Fig. 7a with b, it is also found that for all the dehydriding temperatures, $x = 200$ alloy displays faster dehydriding kinetics than $x = 100$ alloy, indicating that increasing Ni content facilitates the improvement in dehydriding kinetics.

3.4 Hydrogen desorption activation energy

Activation energy is viewed as a determined crucial parameter for evaluating the gas–solid reaction kinetics. With regard to gaseous hydrogen desorption, it is generally considered to be associated with total energy barrier concerning hydrogen desorption processes [23]. Hence, the driving force of hydrogen desorption reaction can be determined according to the change in activation energy. So Arrhenius and Kissinger methods were used to calculate the hydrogen desorption activation energy of alloys. The dehydrogenation activation energy (E_a^{de}) can be estimated by Arrhenius method according to the following equation [24]:

$$k = A \exp\left(\frac{-E_a^{\text{de}}}{RT}\right) \quad (6)$$

where A is a temperature-independent coefficient, T is the absolute temperature and k is an effective kinetic parameter. The hydrogen desorption curves were analyzed using Johnson–Mehl–Avrami (JMA) equation [25, 26]:

$$\ln[-\ln(1 - \alpha)] = \eta \ln k + \eta \ln t \quad (7)$$

where α is the phase fraction transformed at time t which can be identified with a normalized hydrogen content (ranging from 0 to 1) and η is the Avrami exponent. Based on the data in Fig. 7, the logarithmic transform of the Eq. (5) was used to construct a graph of $\ln[-\ln(1 - \alpha)]$ versus $\ln t$ at 553, 573, 593 and 613 K in which isothermal experimental data are found to be approximately linear, as illustrated in Fig. 8. The linear fitting can be done by plotting $\ln k$ versus $1/T$, which is also shown in Fig. 8. From the slope of the Arrhenius plot of $\ln k$ versus $1/T$, the activation energy (E_a^{de}) can be easily calculated. The E_a^{de} values of as-milled (5 h) LaMg₁₁Ni + x wt% Ni ($x = 100, 200$)

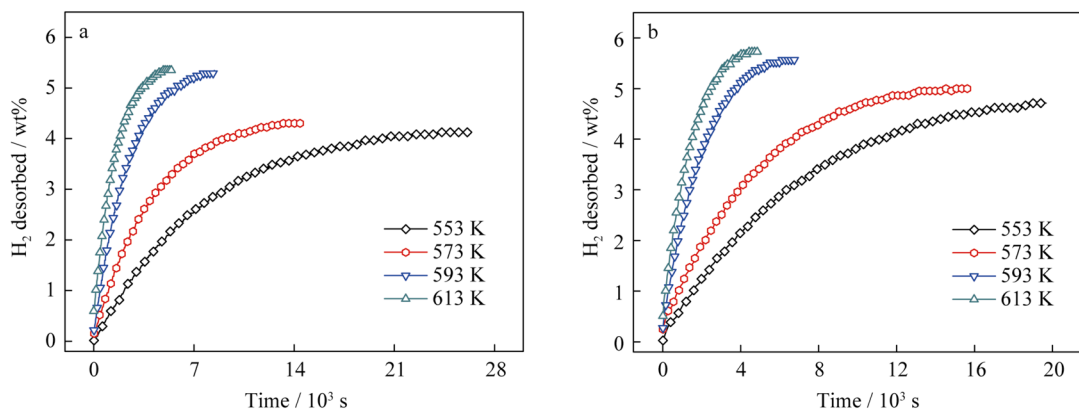


Fig. 7 Hydrogen desorption kinetic curves of as-milled (5 h) LaMg₁₁Ni + x wt% Ni ($x = 100, 200$) alloys at 553, 573, 593 and 613 K: **a** $x = 100$ and **b** $x = 200$

alloys are 86.7 and 74.2 kJ·mol⁻¹, respectively. Evidently, increasing Ni content can markedly decrease the hydrogen desorption activation energy of LaMg₁₁Ni alloys.

Another method to calculate the activation energy is the Kissinger one, and Kissinger equation is as follows [27]:

$$\frac{d[\ln(\beta/T_p^2)]}{d(1/T_p)} = \frac{-E_k^{\text{de}}}{R} \quad (6)$$

where E_k^{de} is activation energy, β is the heating rate and T_p is the absolute temperature corresponding to the maximum desorption rate in DSC curves. To meet the calculation requirement of Kissinger method, the hydrogen desorption reaction of as-milled (5 h) LaMg₁₁Ni + x wt% Ni ($x = 100, 200$) alloys which have absorbed hydrogen at 573 K and 3 MPa was measured by DSC at heating rates of 5, 10, 15 and 20 K·min⁻¹, respectively, as demonstrated in Fig. 9. A clear endothermic peak is observed in correspondence with the hydrogen desorption. Furthermore, all the alloys are found to display similar peak shapes, suggesting that each reaction is involved in the same reaction process. Meanwhile, by comparing Fig. 9a with b, it is found that for each heating rate, the endothermic peak of $x = 200$ alloy has a drift to low temperature, indicating that the reaction rate is ameliorated by increasing Ni content in the hydrogen desorption process as well. Based on the data in Fig. 9, the logarithmic transform of Eq. (6) was used to plot a graph of $\ln(\beta/T_p^2)$ versus $1/T_p$, namely Kissinger plots, which are found to be approximately linear, as shown in Fig. 9. From the slope of Kissinger plot, the activation energy (E_k^{de}) can be easily calculated. The E_k^{de} values of as-milled (5 h) LaMg₁₁Ni + x wt% Ni ($x = 100, 200$) alloys are 78.6 and 71.2 kJ·mol⁻¹, respectively.

To establish the relationship between the hydrogen activation energy of alloys and milling time, the hydrogen

desorption activation energies of all as-milled LaMg₁₁-Ni + x wt% Ni ($x = 100, 200$) alloys using Arrhenius and Kissinger methods were calculated, to obtain the milling time dependence of E^{de} (for Arrhenius method $E^{\text{de}} = E_a^{\text{de}}$; for Kissinger method $E^{\text{de}} = E_k^{\text{de}}$) values of the alloys, as described in Fig. 10. It is found that the activation energies calculated by the two methods both decrease with milling time increasing, suggesting that the enhancement of the hydrogen desorption kinetics which results from extending milling time originates from a decrease in the activation energy. Moreover, no matter which method, increasing Ni content decreases the hydrogen desorption activation energy, meaning that increasing Ni content obviously facilitates the amelioration of hydrogen desorption kinetics of the alloys. Furthermore, by comparing the results calculated by Arrhenius and Kissinger methods, it can be found that the activation energy derived by Arrhenius method is larger than that by Kissinger method, which is most likely ascribed to the change in hydrogen desorption reaction mechanism. A very similar result was reported by Baricco et al. [28].

Some elucidations can be provided for the effects of Ni content and milling time on the hydrogen absorption and desorption kinetics of the alloys. As for the positive contribution of the mechanical milling to hydrogen storage kinetics, it may be attributed to a change in the alloy structure which results from the ball milling. The crystalline alloy milled mechanically becomes at least partially disordered and its structure changes into nanocrystalline or amorphous, creating a lot of new crystallites and grain boundaries (Fig. 3), which can provide numerous sites with low diffusion activation energy, thus facilitating the diffusion of hydrogen atoms in alloys [29]. Here, it is noteworthy that ball milling for a higher time of 20 h for $x = 100$ alloy or 10 h for $x = 200$ alloy will incur an undesirable decrease in the hydriding rate caused by the

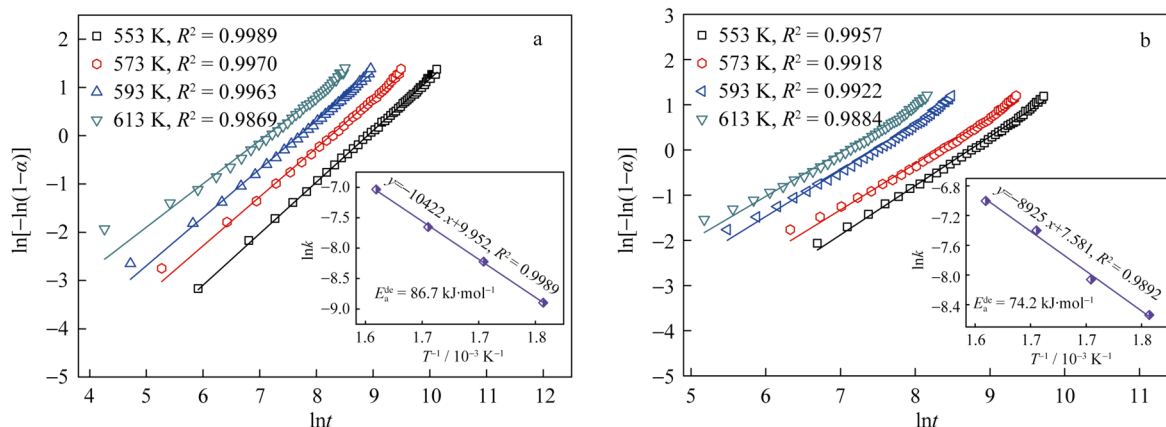


Fig. 8 Plots of $\ln[-\ln(1-\alpha)]$ versus $\ln t$ of as-milled (5 h) LaMg₁₁Ni + x wt% Ni ($x = 100, 200$) alloys at 553, 573, 593 and 613 K and Arrhenius plots (R^2 , degree of fitting): **a** $x = 100$ and **b** $x = 200$

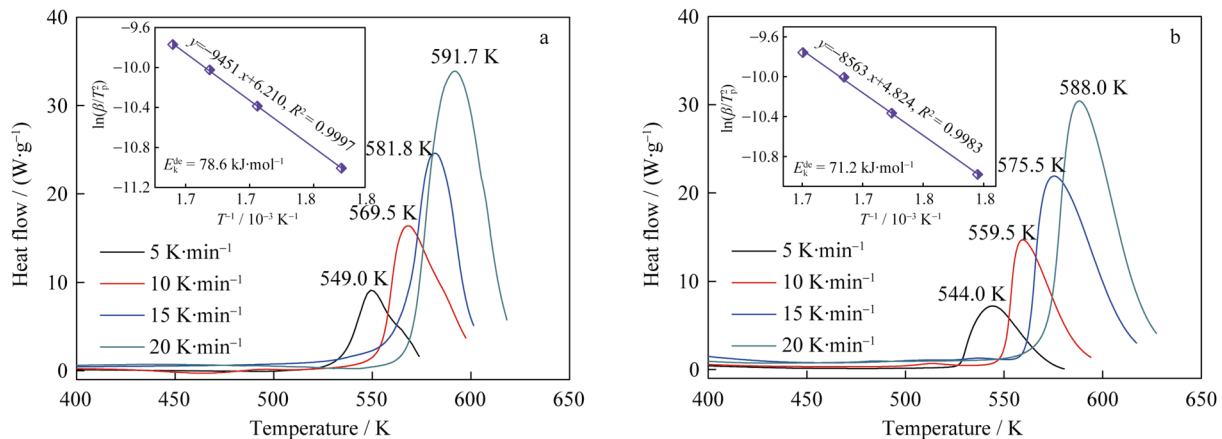


Fig. 9 DSC curves of as-milled (5 h) LaMg₁₁Ni + *x* wt% Ni (*x* = 100, 200) alloys at various heating rates and Kissinger plots: **a** *x* = 100 and **b** *x* = 200

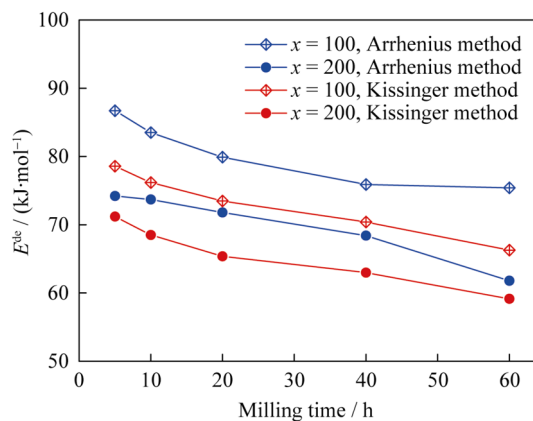


Fig. 10 Variations of hydrogen desorption activation energies of as-milled LaMg₁₁Ni + *x* wt% Ni (*x* = 100, 200) alloys calculated by Arrhenius and Kissinger methods with milling time

addition of Ni facilitating the glass forming, because the diffusion ability of hydrogen atoms in an amorphous phase is much lower than that in a nanocrystalline phase [30]. As to the positive action of increasing milling time on the hydrogen desorption kinetics, it is now well established that reducing the grain size far below the micrometer scale can dramatically improve the dehydrogenation properties of Mg-based alloys [31]. The improved hydrogen absorption and desorption kinetics by increasing Ni content is believed to create relatively catalytic alloy surface for the hydrogen reactions during mechanical milling [32].

4 Conclusion

The variation of Ni content incurs a very slight effect on the thermodynamic parameters (ΔH and ΔS) of as-milled LaMg₁₁Ni + *x* wt% Ni (*x* = 100, 200) alloys, whereas it dramatically improves hydrogen absorption and desorption

kinetics of alloys, for which the decreased hydrogen desorption activation energy caused by increasing Ni content is basically responsible. Gaseous hydrogen absorption capacity (C_{100}^a) and kinetics (R_{10}^a) of alloys have maximum values with milling time varying, but hydrogen desorption kinetics (R_{20}^d) always increases with milling time prolonging, which is due to the facilitated glass forming ability by increasing Ni content and the decreased hydrogen desorption activation energy caused by extending milling time. Arrhenius and Kissinger methods were used to evaluate the hydrogen desorption activation energy of as-milled alloy. The results reveal that increasing Ni content and prolonging milling time can markedly lower the hydrogen desorption activation energy, which is responsible for the improvement in the hydrogen desorption kinetics of as-milled alloys.

Acknowledgements This study was financially supported by the National Natural Science Foundation of China (Nos. 51371094 and 51471054).

References

- [1] Mori D, Hirose K. Recent challenges of hydrogen storage technologies for fuel cell vehicles. *Int J Hydrogen Energy*. 2009; 34(10):4569.
- [2] Schlapbach L, Züttel A. Hydrogen-storage materials for mobile applications. *Nature*. 2001;414(6861):353.
- [3] Zhang YH, Chen LC, Yang T, Xu C, Ren HP, Zhao DL. The electrochemical hydrogen storage performances of Si-added La–Mg–Ni–Co-based A₂B₇-type electrode alloys. *Rare Met*. 2015;34(8):569.
- [4] Li WB, Li L, Ren QL, Wang YJ, Jiao LF, Yuan HT. Ni–B-doped NaAlH₄ hydrogen storage materials prepared by a facile two-step synthesis method. *Rare Met*. 2015;34(9):679.
- [5] Zhao DL, Zhang YH. Research progress in Mg-based hydrogen storage alloys. *Rare Met*. 2014;33(5):499.
- [6] Poletaev AA, Denys RV, Solberg JK, Tarasov BP, Yartys VA. Microstructural optimization of LaMg₁₂ alloy for hydrogen storage. *J Alloys Compd*. 2011;509S(2):S633.

- [7] Lv YJ, Zhang B, Wu Y. Effect of Ni content on microstructural evolution and hydrogen storage properties of Mg- x Ni-3La ($x = 5, 10, 15, 20$ at.%) alloys. *J Alloys Compd.* 2015;641(2):176.
- [8] Paskaš Mamula B, Grbović Novaković J, Radisavljević I, Ivanović N, Novaković N. Electronic structure and charge distribution topology of MgH₂ doped with 3d transition metals. *Int J Hydrogen Energy.* 2014;39(11):5874.
- [9] Jain IP, Lal C, Jain A. Hydrogen storage in Mg: a most promising material. *Int J Hydrogen Energy.* 2010;35(10):5133.
- [10] Gennari FC, Esquivel MR. Structural characterization and hydrogen sorption properties of nanocrystalline Mg₂Ni. *J Alloys Compd.* 2008;459(1–2):425.
- [11] Spassov T, Lyubenova L, Köster U, Baró MD. Mg–Ni–RE nanocrystalline alloys for hydrogen storage. *Mater Sci Eng A.* 2004;375–377:794.
- [12] Wirth E, Milcius D, Filiou C, Noréus D. Exploring the hydrogen sorption capacity of Mg–Ni powders produced by the vapour deposition technique. *Int J Hydrogen Energy.* 2008;33(12):3122.
- [13] Løken S, Solberg JK, Maehlen JP, Denys RV, Lototsky MV, Tarasov BP, Yartys VA. Nanostructured Mg–Mm–Ni hydrogen storage alloy: structure–properties relationship. *J Alloys Compd.* 2007;446–447:114.
- [14] Gu H, Zhu YF, Li LQ. Effect of La/Ni ratio on hydrogen storage properties of Mg–Ni–La system prepared by hydriding combustion synthesis followed by mechanical milling. *Int J Hydrogen Energy.* 2008;33(12):2970.
- [15] Zhang QA, Jiang CJ, Liu DD. Comparative investigations on the hydrogenation characteristics and hydrogen storage kinetics of melt-spun Mg₁₀NiR (R = La, Nd and Sm) alloys. *Int J Hydrogen Energy.* 2012;37(14):10709.
- [16] Wang Y, Wang X, Li CM. Electrochemical hydrogen storage properties of ball-milled NdMg₁₂ alloy with Ni powders. *Int J Hydrogen Energy.* 2008;33(3):1023.
- [17] Poletaev AA, Denys RV, Maehlen JP, Solberg JK, Tarasov BP, Yartys VA. Nanostructured rapidly solidified LaMg₁₁Ni alloy: microstructure, crystal structure and hydrogenation properties. *Int J Hydrogen Energy.* 2012;37(4):3548.
- [18] Cao ZJ, Ouyang LZ, Wu YY, Wang H, Liu JW, Fang F, Sun DL, Zhang QG, Zhu M. Dual-tuning effects of In, Al, and Ti on the thermodynamics and kinetics of Mg₈₅In₅Al₅Ti₅ alloy synthesized by plasma milling. *J Alloys Compd.* 2015;623:354.
- [19] Abdellaoui M, Mokbli S, Cuevas F, Latroche M, Percheron-Guégan A, Zarrouk H. Structural and electrochemical properties of amorphous rich Mg_xNi_{100-x} nanomaterial obtained by mechanical alloying. *J Alloys Compd.* 2003;356–357:557.
- [20] Denys RV, Poletaev AA, Solberg JK, Tarasov BP, Yartys VA. LaMg₁₁ with a giant unit cell synthesized by hydrogen metallurgy: crystal structure and hydrogenation behavior. *Acta Mater.* 2010;58(7):2510.
- [21] Falahati H, Barz DPJ. Evaluation of hydrogen sorption models for AB₅-type metal alloys by employing a gravimetric technique. *Int J Hydrogen Energy.* 2013;38(21):8838.
- [22] Anik M, Karanfil F, Küçükdeveci N. Development of the high performance magnesium based hydrogen storage alloy. *Int J Hydrogen Energy.* 2012;37(1):299.
- [23] Sadhasivam T, Hudson MSL, Pandey SK, Bhatnagar A, Singh MK, Gurunathan K, Srivastava ON. Effects of nano size mischmetal and its oxide on improving the hydrogen sorption behaviour of MgH₂. *Int J Hydrogen Energy.* 2013;38(18):7353.
- [24] Laidler KJ. A glossary of terms used in chemical kinetics, including reaction dynamics. *Pure Appl Chem.* 1996;68(1):149.
- [25] Avrami M. Kinetics of phase change. I General theory. *J Chem Phys.* 1939;7(12):1103.
- [26] Fernández JF, Sánchez CR. Simultaneous TDS–DSC measurements in magnesium hydride. *J Alloys Compd.* 2003;356–357:348.
- [27] Kissinger HE. Reaction kinetics in differential thermal analysis. *Anal Chem.* 1957;29(11):1702.
- [28] Baricco M, Rahman MW, Livraghi S, Castellero A, Enzo S, Giamello E. Effects of BaRuO₃ addition on hydrogen desorption in MgH₂. *J Alloys Compd.* 2012;536:S216.
- [29] Wu Y, Han W, Zhou SX, Lototsky MV, Solberg JK, Yartys VA. Microstructure and hydrogenation behavior of ball-milled and melt-spun Mg–10Ni–2Mm alloys. *J Alloys Compd.* 2008;466(1–2):176.
- [30] Xie DH, Li P, Zeng CX, Sun JW, Qu XH. Effect of substitution of Nd for Mg on the hydrogen storage properties of Mg₂Ni alloy. *J Alloys Compd.* 2009;478(1–2):96.
- [31] Song MY, Yim CD, Kwon SN, Bae JS, Hong SH. Preparation of Mg–23.5Ni–10(Cu or La) hydrogen-storage alloys by melt spinning and crystallization heat treatment. *Int J Hydrogen Energy.* 2008;33(1):87.
- [32] Anik MJ. Electrochemical hydrogen storage capacities of Mg₂Ni and MgNi alloys synthesized by mechanical alloying. *J Alloys Compd.* 2010;491(1–2):565.